Regulating the $NaSe_x$-assisted crystallization of $Cu_2ZnSn(S,Se)_4$ film by modifying the reaction between Na source and Se in the co-selenization process

Chao GAO [1,2,3,4*], Yuzhou SUN [1], Tingchun WU [1], Hao LI [1], Yang LIU [1], Qing ZHOU [1], Zeran GAO [1], Xinzhan WANG [1,2,3,4], Jianjun LI [5,6,*] & Wei YU [1,2,3,4*]

[1] College of Physics Science and Technology, Hebei University, Baoding 071002, China

[2] National & Local Joint Engineering Laboratory for New Energy Opto-electronics Devices, Hebei University, Baoding 071002, China

[3] Province-Ministry Co-construction Collaborative Innovation Center of Hebei Photovoltaic Technology, Hebei University, Baoding 071002, China

[4] Hebei Key Laboratory of Photo-Electricity Information and Materials, Hebei University, Baoding 071002, China

[5] Shenyang National Laboratory for Materials Science, Institute of Metal Research, Chinese Academy of Sciences, Shenyang 110016, China

[6] School of Materials Science and Engineering, University of Science and Technology of China, Shenyang 110016, China

Authors Contribution Statement

Chao Gao: Conceptualization, Supervision Funding acquisition **Yuzhou Sun**: Investigation, Writing – Original Draft **Tingchun Wu**: Investigation, Validation **Hao Li**: Investigation, Resources **Yang Liu:** Resources **Qing Zhou:** Resources **Zeran Gao**: Resources **Xinzhan Wang:** Funding acquisition, **Jianjun Li:** Writing - Review & Editing **Wei Yu**: Project administration, Funding acquisition

* Corresponding authors: Chao Gao (cgao@hbu.edu.cn), Jianjun Li (jjli@imr.ac.cn), Wei Yu (yuwei@hbu.edu.cn)

Abstract

The $NaSe_x$-assisted crystallization plays an important role in determining the photo-electric quality of $Cu_2ZnSn(S,Se)_4$ (CZTSSe) films. However, the method to regulate such process is rarely reported. Herein, a co-selenization process is developed to regulate the $NaSe_x$-assisted crystallization in which different sodium sources are utilized together with Se. By changing the type of the sodium source, the reaction between the sodium source and Se can be altered, which results in $NaSe_x$ flux with different properties. When Na_2S is used as sodium source, $NaSe_x$ with optimum properties can be generated. In this condition, the kinetic process for the growth of the CZTSSe grains can be modified, which helps to improve the defect formation of the film. Moreover, the $NaSe_x$ flux could penetrate the grain-boundaries of the crystallized layer. This can enhance the bottom-to-top diffusion of the elements, thus eliminating the fine-grain layer. By using Na_2S/Se co-selenization, both the defect properties and the morphology of the CZTSSe film are improved. The fabricated CZTSSe solar cells achieve the best efficiency of 12.4% (without anti-reflection coating). This paper clarifies the mechanism of the $NaSe_x$-assisted crystallization, which provides a new route for the crystallization optimization of CZTSSe film.

Keywords: $Cu_2ZnSn(S,Se)_4$; Solar cell; $NaSe_x$-assist crystallization.

1. Introduction

Due to the advantages such as high absorption coefficient, tunable optical bandgap, non-toxic and earth abundant constitution, $Cu_2ZnSn(S,Se)_4$ (CZTSSe) photovoltaic material is expected to has good prospect.[1–4]However, the current efficiency of CZTSSe solar cell (<14.9%) is far below the efficiencies of its counterparts (e.g., 23.6% for $Cu(In,Ga)Se_2$ solar cell).[5,6] Essentially, the poor performances of CZTSSe solar cells are caused by the unfavorable defects in CZTSSe absorber layer. [7,8] To obtain high-efficient CZTSSe solar cell, the defect properties of the CZTSSe film must be optimized. [9–11]

Alkali-metal doping is an effective way to improve the defect properties of CZTSSe film.[12,13] By introducing alkali-metal source (NaF, NaCl, etc) in the precursor film, or using alkali post treatment, alkali-metal elements can be incorporated in CZTSSe film. [14–20]The incorporated alkali-metal atoms can occupy the lattice sites or exist in the grain boundaries of CZTSSe film. Consequently, the lattice defects in CZTSSe grains can be optimized and the defects in the grain boundaries of CZTSSe film can be passivated. [21–25]

Besides, the alkali-metal doping may affect the defect properties of CZTSSe film by altering the crystallization of the film. During the selenization process, liquid alkali-metal chalcogenide could be generated via the reaction between alkali-metal and Se, which can greatly enhance the elemental diffusion in CZTSSe film. [26] As a result, the CZTSSe grains can grow up sufficiently, and the defect properties of the film could be improved by reducing the defective grain-boundaries or the fine-grain layer. [27,28] In addition, the contact between the liquid flux and the CZTSSe grain may modify the kinetic process of the grain-growth. For example, it is reported that the K surfactant on CZTSSe film can prevent the formation of Zn_{Cu} (donor for CZTSSe) in CZTSSe grains.[29] For these reasons, the liquid flux assisted crystallization of CZTSSe film could play important roles in determining the defect properties of the film. It would make sense to investigate the detailed mechanism and explore routes to regulate such process.

In principle, the properties of the liquid flux (melting point, viscosity, etc.) could affect the crystallization of CZTSSe film. It might be possible to regulate the liquid flux assisted crystallization by modifying the properties of the flux. For CZTSSe film, sodium is the most popular alkali-metal element because sodium lime glass (SLG) is usually used as the substrate. Due to the diffusion of sodium from the substrate, or the condense of gaseous $NaSe_x$ (forms via the reaction between Se and SLG glass) on the film, sodium can incorporate in CZTSSe film during the selenization process. [30] According to the Na-Se phase diagram, Se rich environment would be necessary for the generation of liquid $NaSe_x$ flux ($x>1$). [31] Thus, the front surface is the most favorable position for the generation of $NaSe_x$ flux (Na-rich layers are indeed detected on CZTSSe films, which may be the residue of the $NaSe_x$ flux. **Figure S1**). Our previous investigations reveal

that the sodium on the surface of the CZTSSe film mainly results from the condense of the gaseous $NaSe_x$ (see the Supporting Information). In this condition, the generation of the $NaSe_x$ flux could be determined by the formation and condense of the gaseous $NaSe_x$. By adjusting the reaction between Se and the SLG substrate (or other kind of Na-contained matter), the properties of the $NaSe_x$ flux might be modified.

In this paper, co-selenization (i.e., additional sodium source is added together with Se) is used to regulate the $NaSe_x$-assisted crystallization of CZTSSe film.[32] The results reveal that the type of the sodium source can affect the reaction between the sodium source and Se. By this way, the properties of the $NaSe_x$ flux and thereby the $NaSe_x$-assisted crystallization of CZTSSe film can be regulated. Consequently, the properties of the CZTSSe film are altered. It is found Na_2S can act as the optimum sodium source. In the Na_2S/Se co-selenization process, the formation temperature of the $NaSe_x$ flux can be decreased, which can enhance the early-stage crystallization of the film. Moreover, the $NaSe_x$ flux can penetrate the grain boundaries of the top crystallized layer in the co-selenization process. This can eliminate the fine-grain layer by enhancing the bottom-to-top diffusion of the elementals through the grain-boundaries. By using the Na_2S/Se co-selenization process, the morphology and the defect properties of the CZTSSe film, as well as the interfacial properties of the CZTSSSe solar cell are all improved. Consequently, the carrier recombination in CZTSSe solar cell is greatly reduced. The fabricated CZTSSe solar cell achieves the best efficiency of 12.4%. These results would provide a new route for the crystallization regulation of CZTSSe films.

2. Methodology

Non-vacuum solution method was used to prepare CZTSSe films. By successively dissolving 2.3 mmol of $Cu(CH_3COO)_2 \cdot H_2O$, 1.7 mmol of $SnCl_2 \cdot 2H_2O$, 1.6 mmol of $ZnCl_2$, and 5.5 mmol of $CS(NH_2)_2$ in 2 mL of dimethyl sulfoxide (DMSO), the precursor solution was obtained. Then the precursor film was prepared by repeatedly spin-coating the precursor solution on SLG/Mo substrate and drying the wet coating (the thickness of the precursor film was controlled to around 1μm).

The selenization of the film was implemented in a tube furnace. For the conventional selenization, a closed graphite box contained the precursor film and 0.3g of Se pellet was placed in the tube furnace. Then the furnace was evacuated to vacuum and refilled with nitrogen. After that, a specific temperature profile was executed in the furnace to complete the selenization. Additionally, NaCl, NaF, NaOH, Na_2S and $Na_2S_2O_3$ aqueous solutions were prepared, respectively. Then 100 μL of the solution was dropped and dried on quartz glass slide with the area of $4cm^2$ (as sodium source). For the co-selenization, additional sodium source was placed in the graphite box before the selenization process. The other steps of the co-selenization are the same

as that of the conventional selenization. It was found the CZTSSe solar cell exhibited the best performances when the concentration of the Na_2S solution was 0.06 mol/L (**Figure S9**). Therefore, the concentrations for all the solutions were fixed at 0.06 mol/L.

To complete the solar cell fabrication, CdS buffer layer (~50nm) was deposited on CZTSSe film by chemical bath deposition. Then i-ZnO (~50nm) layer and ITO (~200nm) layer were deposited on the buffer layer by sputtering. Finally, Ni/Al metal grids were evaporated on the ITO layer. No anti-reflection coatings were utilized in the CZTSSe solar cells. Before the characterizations, the solar cells were divided into small pieces with the area of 0.2cm^2. The other details for the preparation of CZTSSe films and solar cells can be found in our previous publication. [33,34]

Bruker D8 Advance X-ray diffractometer and JY LabRAM HR Raman spectrometer were used to measure the X-ray diffraction (XRD) patterns and the Raman spectra, respectively. Nova nanoSEM450 scanning electron microscopy was used for morphology and composition measurement. Escalab 250Xi X-ray photoelectron spectroscopy was used to measure the X-ray photoelectron spectra (XPS). Agilent B1500A semiconductor device analyzer was used for the current-voltage (I-V) and capacity-voltage (C-V) measurement. For the I-V measurement, the solar cell was illuminated by a solar simulator which simulates the AM1.5G irradiation. QTesT 1000ADX setup was used to measure the quantum efficiencies (QE) of the solar cell. Keysight E4980A LCR meter was used for the admittance spectroscopy analysis. PGSTAT302N electrochemical workstation was used for the electrochemical impedance spectroscopy measurement.

3. Results and discussions

3.1. Effect of the sodium source on the properties of the CZTSSe films and solar cells

Different CZTSSe films were prepared based on conventional selenization and co-selenization processes. For the co-selenization processes, aqueous solutions contained different sodium sources (NaCl, NaF, NaOH, $Na_2S_2O_3$ or Na_2S) were prepared firstly. Then 100 μL of the solution was dropped and dried on quartz glass slide (4 cm^2). The quartz slides loaded with the sodium sources were used together with Se for the co-selenization processes. The CZTSSe films based on conventional selenization was named as W/O-Na, while the CZTSSe films selenized with additional NaCl, NaF, NaOH, $Na_2S_2O_3$, Na_2S are named as W-NaCl, W-NaF, W-NaOH, W-$Na_2S_2O_3$, W-Na_2S, respectively. The other details for the preparation can be found in the experimental details of this paper.

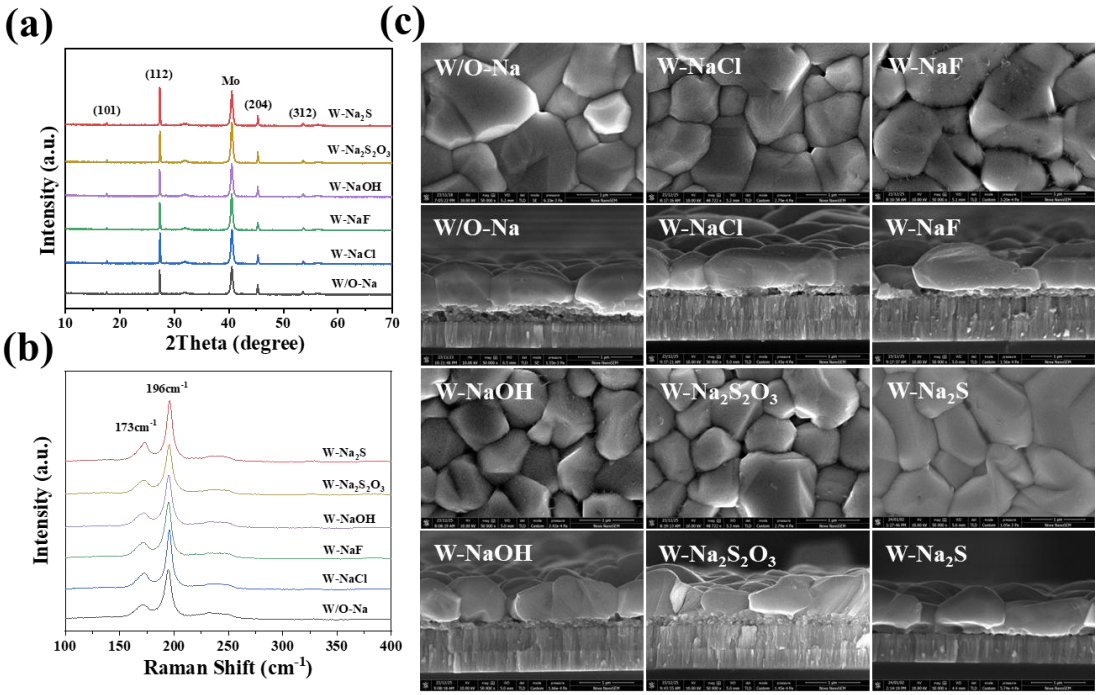

Figure 1. XRD patterns (a), Raman spectra (b) and SEM images (c) of the CZTSSe films with different selenization conditions.

Figure 1 shows the XRD patterns, the Raman spectra and the SEM images of the CZTSSe films. The compositions of the CZTSSe films are listed in **Table S1**. The XRD patterns and the Raman spectra prove that all the selenized films were mainly constituted by CZTSSe. From the normalized Raman spectra of the CZTSSe films (**Figure S3**) it is found the Raman peak at 196 cm^{-1} becomes narrower when additional sodium source is used for the selenization (the W-Na_2S film exhibits the narrowest Raman peak). This result indicates that the co-selenization process can increase the crystallinity of the CZTSSe film. As the variation of the Raman modes can reflect the changes of the defects in CZTSSe material, the defect properties of the CZTSSe films are analyzed based on the normalized Raman data (**Figure S3**). [35] Compared to the conventional selenization, the formation of Zn_{Cu} and Sn_{Zn} defects in CZTSSe film can be suppressed by the co-selenization processes (especially for the W-Na_2S film). Besides, the widths and the relative intensities of the Raman peaks are different among the co-selenized CZTSSe films. Thus, the crystallinity and the defect properties of the CZTSSe films can be altered by changing the type of the sodium source in the co-selenization process.

The SEM images show the different morphologies of the CZTSSe films (**Figure 1(c)**). For W/O-Na film, an obvious fine-grain layer exists at the bottom of the film. As a comparison, the thickness of the fine-grain layer is decreased in the co-selenized films (especially, the fine-grain layer is eliminated in W-Na_2S film). Besides, the sizes of the crystalline grains are different among the CZTSSe films (the grain sizes of W-NaOH

and W-$Na_2S_2O_3$ films are obviously smaller than that of the other films). Since the crystallinity, the lattice defects and the morphology are all determined by the crystallization of the film, the results above imply that the kinetic processes of the crystallizations are different among the CZTSSe films (could be caused by the different sodium sources).

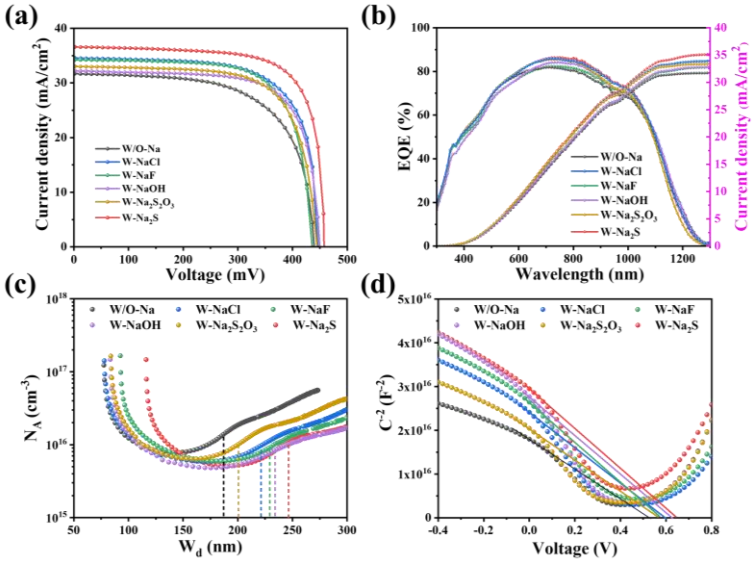

Figure 2. I-V curves (a) and QE curves (b) of the best CZTSSe solar cells; the doping profiles (c) and the build-in potentials (d) in the solar cells.

Figure 2 shows the I-V curves, the QE curves and the C-V analyses of the best CZTSSe solar cell. The device parameters that derived from the data are listed in **Table 1** (the statistics of the parameters for all the solar cells can be seen in **Figure S4**). Compared to the conventional selenization, the co-selenization can reduce the Urbach tail energy (E_u) of the absorber layer, increase the build-in potential (V_{bi}) and the depletion region width (W_d) of the solar cell. For these reasons, the efficiencies of the CZTSSe solar cells are increased by the co-selenization processes. [36] Besides, the CZTSSe solar cells based on different co-selenization processes exhibit different performances. When Na_2S is used as sodium source, the CZTSSe solar cells achieve the best efficiency of 12.4%. These results clearly prove that the type of the sodium source in the co-selenization process can affect the performances of the CZTSSe solar cell.

The results above indicate that the sodium source may affect the crystallization and the properties of the CZTSSe film. During the co-selenization process, the sodium source is separated from the CZTSSe film. Therefore, the sodium source cannot directly act on the crystallization of CZTSSe films. However, gaseous $NaSe_x$ could be generated via the reaction between Se and Na-contained matter (SLG glass and the sodium sources) in the selenization process. [30] The gaseous $NaSe_x$ can condense on the CZTSSe films and evolve

to liquid $NaSe_x$ flux under Se-rich environment. Accordingly, the grain growth in CZTSSe film could be enhanced because the liquid flux can promote the diffusion of the elements (mechanism are illustrated and explained in **Figure S2** and the Supporting Information). By this way, the sodium source can influence the crystallization of CZTSSe film even it is separated from the film.

Table 1. Device parameters for the best CZTSSe solar cells

Sample	V_{OC} (V)	J_{SC} (mA/cm^2)	FF (%)	Eff (%)	E_g (eV)	N_{cv} (cm^{-3})	W_d (nm)	V_{bi} (V)	E_u (meV)
W/O-Na	0.436	31.8	64.9	9.0	1.04	1.5 E16	190	0.524	27.4
W-NaCl	0.436	34.5	71.2	10.9	1.04	9.5 E15	220	0.594	26.5
W-NaF	0.426	34.2	72.8	10.6	1.04	9.3 E15	230	0.570	26.7
W-NaOH	0.446	32.2	72.3	10.4	1.05	8.6 E15	236	0.621	25.9
W-Na_2S_2O	0.436	33.0	71.6	10.3	1.06	1.1 E16	203	0.560	26.1
W-Na_2S	0.456	36.6	74.4	12.4	1.05	1.0 E16	243	0.643	25.5

Compared to the conventional selenization, additional sodium source is added in the co-selenization. In this condition, extra reaction (i.e., the reaction between Se and the sodium source) would occur except for the reaction between Se and the SLG substrate. Moreover, the different chemical properties of the sodium sources may cause different reactions between Se and the sodium sources. These may modify the formation of the gaseous $NaSe_x$, as well as the generation of the $NaSe_x$ flux. Therefore, the properties of the $NaSe_x$ flux could be different among the co-selenization processes. With modified properties of the $NaSe_x$ flux, the crystallization and the properties of the CZTSSe film would be changed.

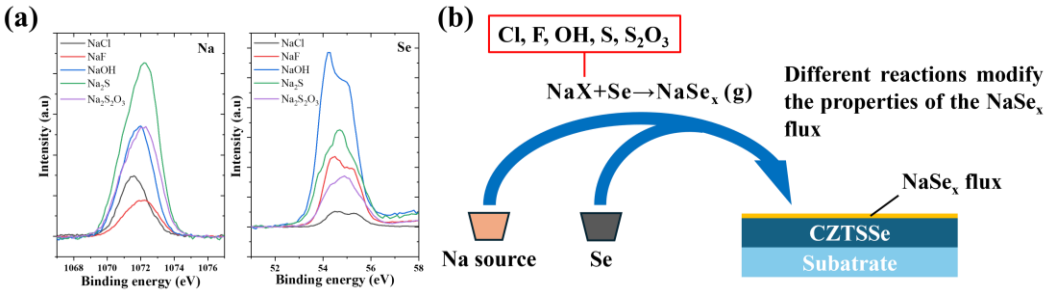

Figure 3. XPS characterization on quartz glass after simulated co-selenization (a); illustration for the generation of $NaSe_x$ flux in the co-selenization process.

To verify whether the reaction between the sodium source and Se is affected by the type of the sodium

source, the compositions of the sodium sources are measured after the co-selenization processes (**Figure S5, Table S2**). For all the residues of the sodium sources, Se can be detected but their compositions are obviously different. These results suggest that the reactions between the sodium sources and Se, as well as the formation of the gaseous $NaSe_x$ are different in the co-selenization processes. To testify whether $NaSe_x$ can be condensed on the CZTSSe film, quartz glass slides are used to simulate the co-selenization processes. After the selenization processes, the surfaces of the quartz slides are characterized by XPS (**Figure 3(a)**). For all the quartz slides, both Na and Se can be detected on their surfaces. These results demonstrate that $NaSe_x$ can be condensed on the quartz glass in the co-selenization process. In addition, it is found the Na XPS peaks locate at different positions of the XPS spectra, and the intensity ratios between the Na peaks and the Se peaks vary among the XPS spectra. Thus, the condensed $NaSe_x$ on the quartz slides could have different compositions and chemical properties. Similarly, it is expected that $NaSe_x$ with different properties are condensed on CZTSSe films in the co-selenization processes. In the high-temperature and Se-rich environment, the condensed $NaSe_x$ may evolve to liquid flux with different properties. By selecting the optimum sodium source (Na_2S), the properties of the $NaSe_x$ flux could be optimized. Accordingly, the $NaSe_x$-assisted crystallization and the properties of the CZTSSe film are improved.

3.2. Crystallization mechanism of CZTSSe films with Na_2S/Se co-selenization

The results above suggest that the crystallization of CZTSSe film can be improved by the co-selenization process. Especially, when Na_2S is used as sodium source, the crystallinity, the defect properties and the morphology of the film are all improved. To clarify the crystallization mechanism of the CZTSSe film, half-selenized films were prepared at different temperatures (with conventional selenization and Na_2S/Se co-selenization). By characterizing the morphologies and constitutions of the half-selenized films, the crystallizations of the CZTSSe films are analyzed.

The XRD patterns, the Raman spectra and the SEM images of the half-selenized films are shown in **Figure 4**. The compositions of the half-selenized films are listed in **Table S3** and **Table S4**. Generally, the films with conventional selenization and Na_2S/Se co-selenization exhibit similar constitution and morphology evolutions. At 300ºC and 350ºC, the XRD patterns and the Raman spectra of the half-selenized films are all dominated by the characteristic peaks of Cu_2ZnSnS_4 (CZTS). At around 400ºC, the characteristic peaks of CZTSSe emerge in the XRD patterns and the Raman spectra. Then with the increase of temperature, the characteristic peaks of CZTS gradually become weak, while the characteristic peaks of CZTSSe gradually become strong. SEM images show that tiny crystalline grains appear in the film when the temperature reach

400ºC. Then the sizes of the crystalline grains and the thickness of the crystallized layers increase as the rise of the temperature.

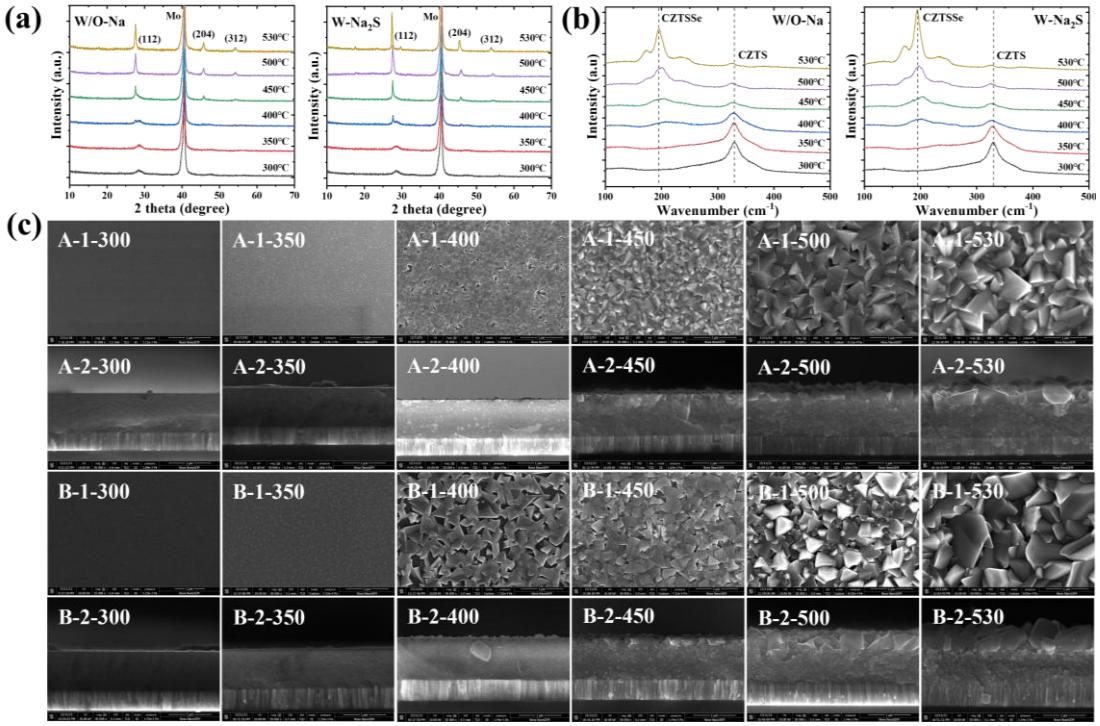

Figure 4. XRD patterns (a), Raman spectra (b) and SEM images (c) of the half-selenized CZTSSe films (A for W/O-Na film and B for W-Na_2S film).

However, the comparisons between the films that selenized at the same temperatures reveal that the utilization of Na_2S can change the crystallization of the film. Compared to that of the W/O-Na film, the characteristic peaks are strengthened in the XRD patterns and Raman spectra of the W-Na_2S film (**Figure 4(a,b)**, **Figure S6**). Besides, the sizes of the crystalline grains are enlarged in W-Na_2S film (especially at 400ºC-450ºC). These results indicate that the early-state crystallization of the CZTSSe film is enhanced by the utilization of Na_2S. XPS characterizations on the half-selenized W-Na_2S film reveal that sodium can emerge on the film at 400ºC. But for W/O-Na film, sodium can only be detected until the temperature reach 530ºC (**Figure S7**). These results imply that the formation temperature of the $NaSe_x$ flux can be reduced in the Na_2S/Se co-selenization process. With the assistance of the $NaSe_x$ flux, the quality of the initial crystalline grains could be improved (e.g., less defects are generated).

The grain-growth of the CZTSSe films mainly occur at high temperature (>500 ºC), which is believed caused by the $NaSe_x$ flux (i.e., $NaSe_x$-assisted crystallization). [37] To analyze the $NaSe_x$-assisted crystallization, a model has been developed based on our experimentals (**Figure S2**). At high temperature,

$NaSe_x$ flux can cover the surface of CZTSSe film. Due to the high chemical potentials, the elements in small grains can be dissolved in the $NaSe_x$ flux. Then the elements are transferred and deposited on the large grains (in which the elements have low chemical potentials) through the $NaSe_x$ flux. Accordingly, rapid grain-growths are achieved with the assistance of $NaSe_x$ flux. However, the transfer of the elements from small grains to large grains can only lead to the growth of the CZTSSe grains but cannot increase the thickness of the crystallized layer (because the total quantity of the atoms in the crystallized layer is not increased). This conflicts with the real condition. To solve this problem, it is believed that the elements that in the bulk of the film can diffuse to the surface through the grain-boundaries. [38] Only by this way, the thickness of the crystallized layer can be increased, and the thickness of the fine-grain layer can be decreased.

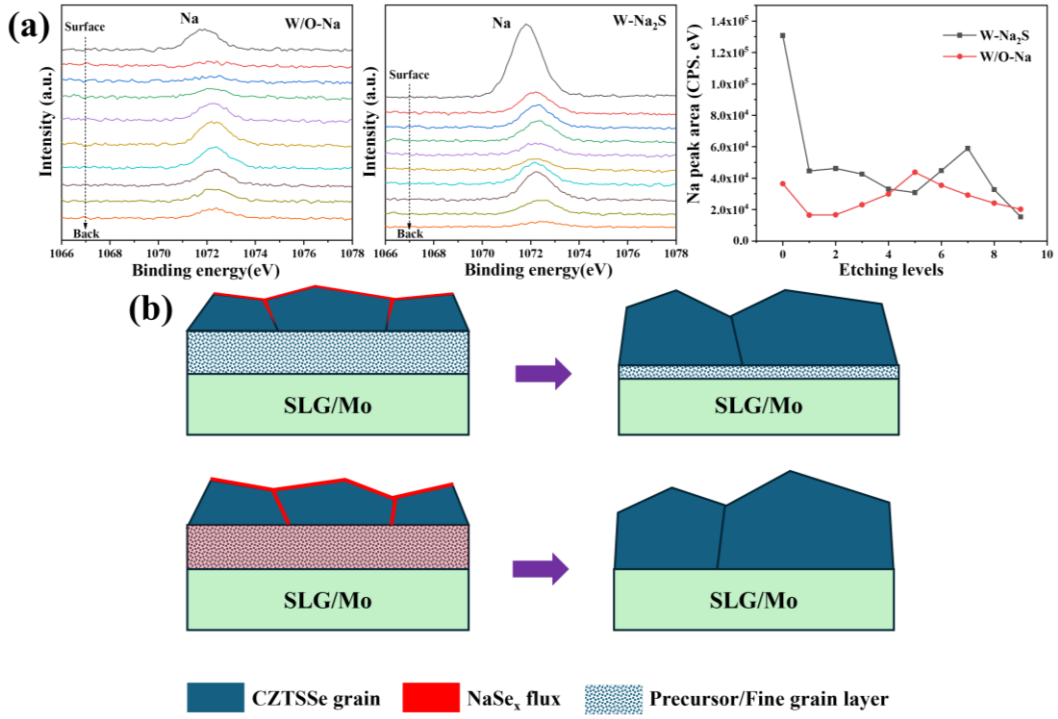

Figure 5. The Na XPS depth profiles in W/O-Na and W-Na_2S films (a); crystallization mechanisms for the W/O-Na and W-Na_2S films (b).

Based on the model above, the different crystallization behaviors of the CZTSSe films in high temperature region can be analyzed. For W/O-Na film, the fine-grain layer remains in the film after selenization (**Figure 1(c)**). This result suggests that the bottom-to-top elemental diffusion is suppresses in the late-stage crystallization of the W/O-Na film (probably due to the reduced grain-boundaries and increased thickness of the crystallized layer). In contrast, the fine-grain layer is eliminated in W-Na_2S film, indicating that the elemental diffusion through the grain-boundaries can be maintained by some way. In **Figure S8**,

liquid-like residue which contained sodium is found at the grain boundary of W-Na_2S film. This indicates that the $NaSe_x$ flux may penetrate the grain-boundaries of the top crystallized layer in the co-selenization process (might be caused by the modified properties of the $NaSe_x$ flux). Besides, the depth Na XPS profiles of W/O-Na and W-Na_2S films (**Figure 5(a)**) reveal that more sodium exist in the surficial region (corresponding to the large-grain layer) of the W-Na_2S film than the W/O-Na film. Due to the large ionic radius, sodium tend to exist in the grain boundaries rather than in the bulk of CZTSSe grains.[39] Therefore, the top crystallized layer in W-Na_2S would contained more sodium at the grain-boundaries, which might be the residue of the $NaSe_x$ flux. With the assistance of the $NaSe_x$ flux at the grain-boundaries, the bottom-to-top diffusion of the elements could be enhanced, which helps to eliminate the fine-grain layer.

As a summary, the crystallization mechanisms of the W/O-Na and the W-Na_2S films in high temperature region are illustrated in **Figure 5(b)**. For W/O-Na film, $NaSe_x$ flux can be generated on the film at temperature above 500ºC. With the assistance of the $NaSe_x$ flux, the rapid growth of the CZTSSe grains can be achieved. However, as the increase of the grain sizes and the thickness of the crystallized layer, the bottom-to-top elemental diffusion gets more and more hard. Eventually, the fine-grain layer remains at the bottom of the film. By adding Na_2S for the selenization, the properties of the $NaSe_x$ flux can be altered. Therefore, the $NaSe_x$ flux could penetrate the grain-boundaries of the crystallized layer. This can maintain the bottom-to-top elemental diffusion and eliminate the fine-grain layer. In addition, the modified properties of the $NaSe_x$ flux may change the kinetic process of the crystallization, thus improving the crystallinity and the defect properties of the film (e.g., suppressing the deep level Sn_{Zn} defect).

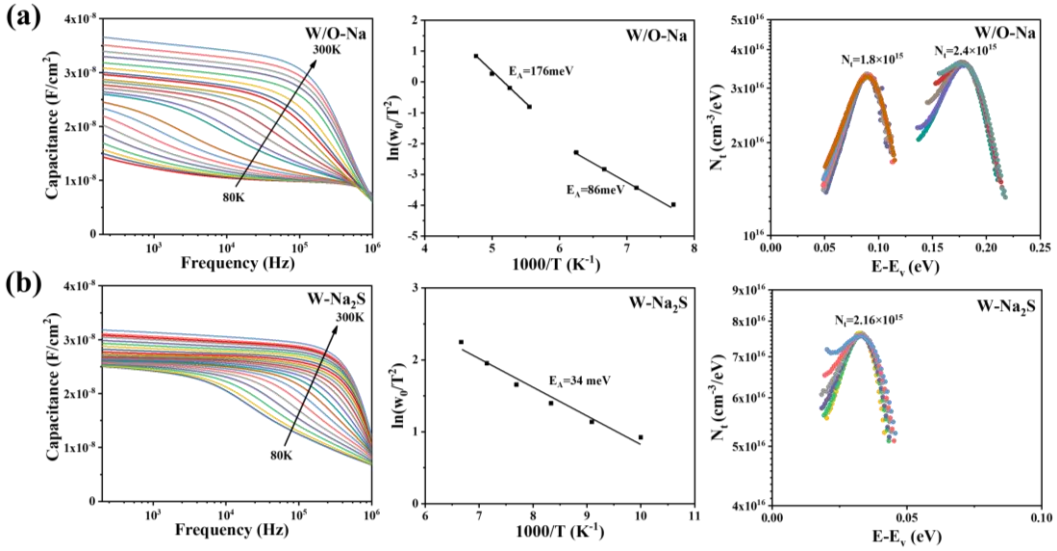

Figure 6. The admittance spectra, the Arrhenius plots and the defect density of the W/O-Na (a) and W-Na_2S (b) solar cells.

3.3. Properties of the CZTSSe film and solar cell based on Na_2S/Se co-selenization

By using the Na_2S/Se co-selenization, the Urbach tail energy of the film can be decreased, and the Sn_{Zn} defect can be reduced. Except that, the Na_2S/Se co-selenization can promote the generation of the shallow level acceptors. **Figure 6** shows the admittance spectra of the CZTSSe solar cells. Based on the data, the Arrhenius plots and the defect spectra can be derived. The estimated energy levels for the acceptors in W/O-Na film are 174 meV and 86 meV, which may be attributed to the Zn_{Sn} and V_{Zn} defects, respectively. As a comparison, acceptor with shallow level (34 meV, could be attributed to V_{Cu} defect) is detected in W-Na_2S film.[40–42] As reported in literature, the deep level acceptor in the depletion region may cause serious carrier recombination of the solar cell. [43] Thus, CZTSSe film with shallow level defect would be favorable for high-efficient solar cell.

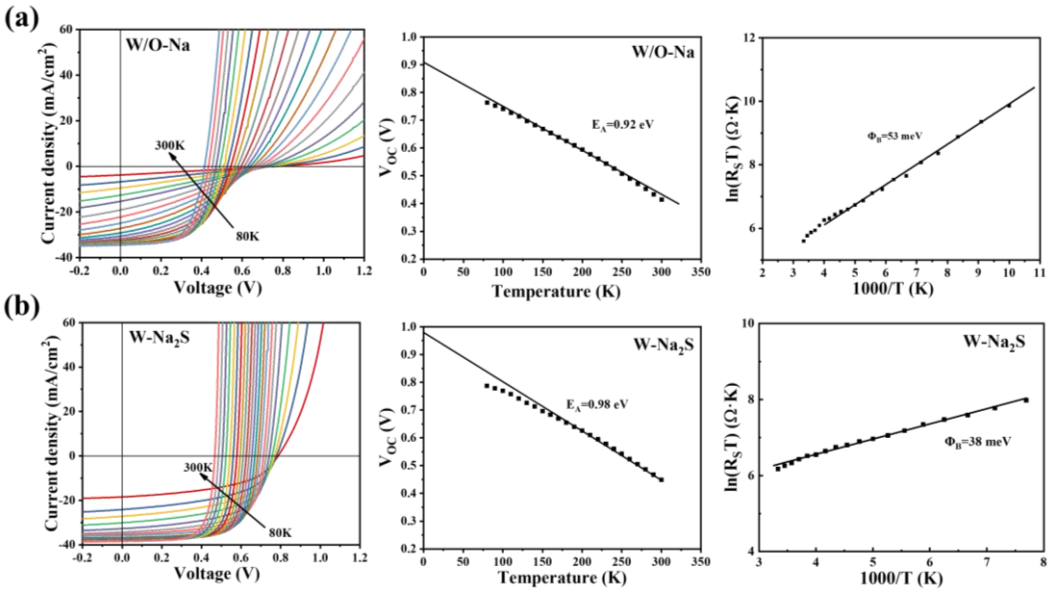

Figure 7. The temperature dependent I-V curves, the estimation of E_R and Φ_B for the W/O-Na (a) and W-Na_2S (b) solar cells.

The different crystallization processes may change the surficial properties of the CZTSSe films, which can consequently modify the interfacial properties of the CZTSSe solar cells. **Figure 7** shows the temperature dependent I-V curves, the estimated excitation energy for the main recombination path (E_R) and the back contact barriers (Φ_B) of the W/O-Na and W-Na_2S solar cells. [44,45] Compared to that of the W/O-Na solar cell, the E_R is increased (from 0.92 eV to 0.98 eV) but the Φ_B is decreased (from 53 meV to 38 meV) for W-Na_2S solar cells. The increased E_R in W-Na_2S solar cell indicates that the band offset at the absorber/buffer

interface is improved, which may be caused by the increased sodium content of the W-Na_2S layer.[46,47] As a result, the recombination around the absorber/buffer interface can be reduced. The decreases Φ_B in W-Na_2S solar cell could be caused by the improved crystallinity of the W-Na_2S film (i.e., the fine-grain layer is eliminated). Therefore, the carrier transportation through the back contact could be enhanced.

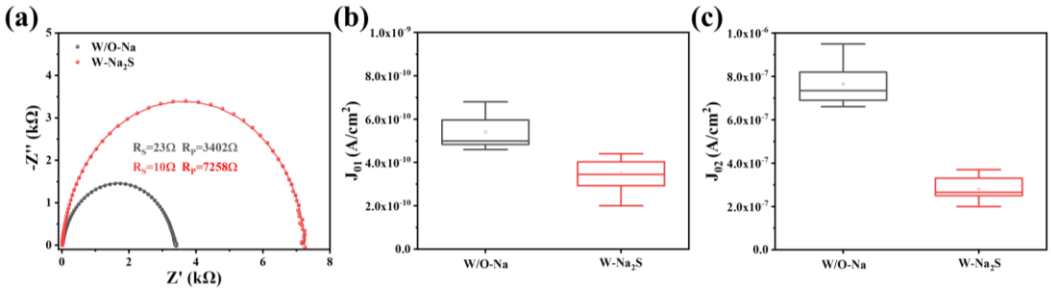

Figure 8. The impedance spectra (a) and the Suns-V_{OC} results (b,c) of the W/O-Na and W-Na_2S solar cells.

Due to the elimination of the defective fine-grain layer, the improved defect properties of the absorber layer, the increased E_R and the reduced Φ_B of the solar cell, the carrier recombination in W-Na_2S solar cell could be suppressed. **Figure 8(a)** shows the electrochemical impedance spectroscopy (EIS) curves of the CZTSSe solar cells. In these curves, the intercept of the curve on real axis represents the series resistance (R_S), while the diameter of the curve equal to recombination resistance (R_P) of the solar cell. [48] The result clearly proves that the carrier recombination in the W-Na_2S solar cell is reduced compared to the W/O-Na solar cell. Besides, Suns-V_{OC} measurement is used to analyze the recombination of the carriers in different regions of the solar cell (**Figure 8(b,c)**). [49] For this measurement, the measured I-V data is fitted by the two-diode model. Thus, two reverse saturation current densities were obtained which can reflect the carrier recombination in quasi-neutral region (J_{01}) and depletion region (J_{02}). Compared to that of the W/O-Na_2S solar cell, both the J_{01} and J_{02} are reduced in W-Na_2S solar cell. This proves that the carrier recombination in both the neutral region and the depletion region are reduced in W-Na_2S solar cell. Because the solar cell performance is substantially determined by the carrier recombination in the solar cell, the reduced carrier recombination in W-Na_2S solar cell would cause enhanced performances of the solar cell.

4. Conclusion

In this paper, the $NaSe_x$-assisted crystallization of CZTSSe film is regulated by using co-selenization process. By changing the type of the sodium source for the co-selenization process, the reaction between the sodium source and Se can be adjusted, which results in $NaSe_x$ flux with different properties. With modified

properties of the $NaSe_x$ flux, the kinetic process of the crystallization in CZTSSe film could be altered. As a result, the crystallinity, the defect properties and the morphology of the CZTSSe film can be changed. It is found Na_2S can act as the optimum sodium source. The utilization of Na_2S could reduce the formation temperature of the $NaSe_x$ flux, which may enhance the early-stage crystallization of the film. Besides, the $NaSe_x$ flux may penetrate the grain-boundaries of the crystallized layer in the co-selenization process. This can facilitate the bottom-to-top elemental diffusion, thereby eliminating the fine-grain layer of the film. Consequently, the CZTSSe film prepared with Na_2S/Se co-selenization process shows uniform morphology, shallow level acceptor (V_{Cu}) and reduced deep level defect (Sn_{Zn}). The fabricated CZTSSe solar cell exhibits increased excitation energy for the main recombination path and reduced back contact barriers. For these reasons, the carrier recombination of the solar cell is significantly reduced. The best CZTSSe solar cell achieves the efficiency of 12.4%.

Acknowledgments

This work was supported by the Natural Science Foundation of Hebei Province (F2023201025), the Hebei Province Optoelectronic Information Materials Laboratory Performance Subsidy Fund Project (No.22567634H), the Open bidding for selecting the best candidates of Baoding (2023chuang206), and the Advanced Talent Incubation Program of Hebei University (521000981316).

References

[1] Y. Zhao, S. Chen, Z. Su, J. Luo, X. Zhang, G. Liang, Research progress of kesterite solar cells, Chin. Sci. Bull. 68 (2023) 4662–4673.

[2] J. Fu, J. Yang, W. Dong, S. Ren, H. Zhu, Y. Wang, J. Hao, J. Wu, R. Wang, D. Zhao, Y. Zhang, Z. Zheng, A critical review of solution-process engineering for kesterite thin-film solar cells: current strategies and prospects, J. Mater. Chem. A 12 (2024) 545–566.

[3] J. Guo, J. Ao, Y. Zhang, A critical review on rational composition engineering in kesterite photovoltaic devices: self-regulation and mutual synergy, J. Mater. Chem. A 11 (2023) 16494–16518.

[4] W. Xie, Q. Yan, Q. Sun, Y. Li, C. Zhang, H. Deng, S. Cheng, A Progress Review on Challenges and Strategies of Flexible $Cu_2ZnSn(S,Se)_4$ Solar Cells, Solar RRL 7 (2023) 2201036.

[5] J. Keller, K. Kiselman, O. Donzel-Gargand, N.M. Martin, M. Babucci, O. Lundberg, E. Wallin, L. Stolt, M. Edoff, High-concentration silver alloying and steep back-contact gallium grading enabling copper indium gallium selenide solar cell with 23.6% efficiency, Nat Energy 9 (2024) 467–478.

[6] Y. Li, C. Cui, H. Wei, Z. Shao, Z. Wu, S. Zhang, X. Wang, S. Pang, G. Cui, Suppressing Element Inhomogeneity Enables 14.9% Efficiency CZTSSe Solar Cells, Advanced Materials 36 (2024) 2400138.

[7] B. Duan, J. Shi, D. Li, Y. Luo, H. Wu, Q. Meng, Underlying mechanism of the efficiency loss in CZTSSe solar cells: Disorder and deep defects, Sci. China Mater. 63 (2020) 2371–2396.

[8] Y. Gong, H. Xin, L. Ding, V_{oc} deficit in kesterite solar cells, J. Semicond. 42 (2021) 100201.

[9] Q. Tian, S. (Frank) Liu, Defect suppression in multinary chalcogenide photovoltaic materials derived from kesterite: progress and outlook, J. Mater. Chem. A 8 (2020) 24920–24942.

[10] D. Shin, B. Saparov, D.B. Mitzi, Defect Engineering in Multinary Earth-Abundant Chalcogenide Photovoltaic Materials, Advanced Energy Materials 7 (2017) 1602366.

[11] H. Wei, Y. Li, C. Cui, X. Wang, Z. Shao, S. Pang, G. Cui, Defect suppression for high-efficiency kesterite CZTSSe solar cells: Advances and prospects, Chemical Engineering Journal 462 (2023) 142121.

[12] X. Zhao, Y. Qi, Z. Zhou, D. Kou, W. Zhou, Y. Meng, S. Yuan, L. Han, S. Wu, Regulating charge carrier recombination in $Cu_2ZnSn(S,Se)_4$ solar cells *via* cesium treatment: bulk and interface effects, J. Mater. Chem. A 11 (2023) 11454–11462.

[13] W. Yang, Y. Ji, W. Chen, Y. Pan, Z. Chen, S. Wu, S.P. Russo, Y. Xu, T.A. Smith, A. Chesman, P. Mulvaney, F. Liu, The Multiple Roles of Na Ions in Highly Efficient CZTSSe Solar Cells, Small 20 (2024) 2307807.

[14] K. Yang, S. Kim, S. Kim, D. Son, J. Lee, Y. Kim, S. Sung, D. Kim, T. Enkhbat, J. Kim, J. Kim, W. Jo, J. Kang, Sodium Effects on the Diffusion, Phase, and Defect Characteristics of Kesterite Solar Cells and Flexible $Cu_2ZnSn(S,Se)_4$ with Greater than 11% Efficiency, Adv Funct Materials 31 (2021) 2102238.

[15] X. Xu, J. Zhou, K. Yin, J. Wang, L. Lou, D. Li, J. Shi, H. Wu, Y. Luo, Q. Meng, 12.84% Efficiency Flexible Kesterite Solar Cells by Heterojunction Interface Regulation, Advanced Energy Materials 13 (2023) 2301701.

[16] L. Dong, S. Tao, M. Zhao, D. Zhuang, Y. Wang, H. Wang, M. Jia, J. Han, H. Zhu, Crystallization mechanism and defect passivation of $Cu_2ZnSn(S,Se)_4$ thin film solar cells *via in situ* potassium doping, J. Mater. Chem. A 11 (2023) 20139–20150.

[17] Q. Sun, C. Shi, W. Xie, Y. Li, C. Zhang, J. Wu, Q. Zheng, H. Deng, S. Cheng, Defect Synergistic Regulations of Li&Na Co-Doped Flexible $Cu_2ZnSn(S,Se)_4$ Solar Cells Achieving over 10% Certified Efficiency, Advanced Science 11 (2024) 2306740.

[18] Y. Yang, X. Kang, L. Huang, S. Wei, D. Pan, Facile and Low-Cost Sodium-Doping Method for High-Efficiency $Cu_2ZnSnSe_4$ Thin Film Solar Cells, J. Phys. Chem. C 119 (2015) 22797–22802.

[19] W. Jeong, K. Kim, J. Kim, H.K. Park, J. Min, J. Lee, S. Mun, S. Kim, J. Jang, W. Jo, D. Lee, Impact of Na Doping on the Carrier Transport Path in Polycrystalline Flexible $Cu_2ZnSn(S,Se)_4$ Solar Cells, Advanced Science 7 (2020) 1903085.

[20] X. Chang, J. Fu, D. Kou, W. Zhou, Z. Zhou, S. Yuan, Y. Qi, Z. Zheng, S. Wu, Synergistic incorporation of NaF and CsF PDT for high efficiency kesterite solar cells: unveiling of grain interior and grain boundary effects, J. Mater. Chem. A 9 (2021) 413–422.

[21] L. Dong, S. Tao, M. Zhao, D. Zhuang, Q. Gong, H. Zhu, Y. Wang, Y. Li, H. Wang, M. Jia, J. Li, Passivation of Grain Boundaries and Defects in CZTSSe Solar Cells by In Situ Na Doping, Solar RRL 7 (2023) 2300061.

[22] A. Jimenez-Arguijo, A. Navarro Güell, Y. Sanchez, C. Malerba, M. Valentini, P. Becker, L. Choubrac, T. Unold, Z. Jehl Li-Kao, S. Giraldo, E. Saucedo, Small Atom Doping: A Synergistic Strategy to Reduce Sn_{Zn} Recombination Center Concentration in $Cu_2ZnSnSe_4$, Solar RRL 6 (2022) 2200580.

[23] M. He, X. Zhang, J. Huang, J. Li, C. Yan, J. Kim, Y. Chen, L. Yang, J.M. Cairney, Y. Zhang, S. Chen, J. Kim, M.A. Green, X. Hao, High Efficiency $Cu_2ZnSn(S,Se)_4$ Solar Cells with Shallow Li_{Zn} Acceptor

Defects Enabled by Solution-Based Li Post-Deposition Treatment, Advanced Energy Materials 11 (2021) 2003783.

[24] X. Zhao, X. Chang, D. Kou, W. Zhou, Z. Zhou, Q. Tian, S. Yuan, Y. Qi, S. Wu, Lithium-assisted synergistic engineering of charge transport both in GBs and GI for Ag-substituted $Cu_2ZnSn(S,Se)_4$ solar cells, Journal of Energy Chemistry 50 (2020) 9–15.

[25] H. Xin, S.M. Vorpahl, A.D. Collord, I.L. Braly, A.R. Uhl, B.W. Krueger, D.S. Ginger, H.W. Hillhouse, Lithium-doping inverts the nanoscale electric field at the grain boundaries in $Cu_2ZnSn(S,Se)_4$ and increases photovoltaic efficiency, Phys. Chem. Chem. Phys. 17 (2015) 23859–23866.

[26] C.M. Sutter-Fella, J.A. Stückelberger, H. Hagendorfer, F. La Mattina, L. Kranz, S. Nishiwaki, A.R. Uhl, Y.E. Romanyuk, A.N. Tiwari, Sodium Assisted Sintering of Chalcogenides and Its Application to Solution Processed $Cu_2ZnSn(S,Se)_4$ Thin Film Solar Cells, Chem. Mater. 26 (2014) 1420–1425.

[27] D. Wang, J. Chen, M. Wu, S. Gao, L. Wu, J. Ao, Y. Sun, Y. Zhang, Synergistic effect of Na and Se on CZTSe solar cells through a soft chemical process, Solar Energy Materials and Solar Cells 198 (2019) 35–43.

[28] Y. Zhao, S. Chen, M. Ishaq, M. Cathelinaud, C. Yan, H. Ma, P. Fan, X. Zhang, Z. Su, G. Liang, Controllable Double Gradient Bandgap Strategy Enables High Efficiency Solution-Processed Kesterite Solar Cells, Advanced Functional Materials 34 (2024) 2311992.

[29] K. Bao, H. Liu, K. Tse, C. Yang, G. Zhong, J. Zhu, Kinetic Processes and Surfactant Design of Group I Elements on the CZTS ($\overline{1}12$) Surface, J. Phys. Chem. C 125 (2021) 376–384.

[30] T. Abzieher, T. Schnabel, M. Hetterich, M. Powalla, E. Ahlswede, Source and effects of sodium in solution-processed kesterite solar cells: Source and effects of sodium in solution-processed kesterite solar cells, Phys. Status Solidi A 213 (2016) 1039–1049.

[31] J. Ma, C. Ji, J. Wang, D. Han, Z. Cui, B. Sa, S. Cui, Critical Evaluation and Thermodynamic Modeling of the Li-Se and Na-Se Binary Systems Using Combined CALPHAD and First-Principles Calculations Method, Metals 12 (2022) 1349.

[32] H. Guo, G. Wang, R. Meng, Y. Sun, S. Wang, S. Zhang, J. Wu, L. Wu, G. Liang, H. Li, Y. Zhang, An efficient Li^+-doping strategy to optimize the band alignment of a $Cu_2ZnSn(S,Se)_4$/CdS interface by a Se&LiF co-selenization process, J. Mater. Chem. A 8 (2020) 22065–22074.

[33] H. Xu, H. Gao, Y. Ma, Q. Zhou, Y. Sun, C. Gao, W. Yu, Boost the Efficiency of $Cu_2ZnSn(S,Se)_4$ Solar Cell by Using Mn^{2+}-Induced Ultrathin CdS Buffer Layer, Solar RRL 7 (2023) 2200984.

[34] Y. Ma, Y. Sun, Z. Zhang, H. Zhao, H. Gao, Q. Zhou, W. Li, X. Teng, C. Gao, W. Yu, Boosting the open-circuit voltage of $Cu_2ZnSn(S,Se)_4$ solar cell by Cd/NH_3 soaking, J. Phys. D: Appl. Phys. 56 (2023) 495103.

[35] M. Dimitrievska, A. Fairbrother, E. Saucedo, A. Pérez-Rodríguez, V. Izquierdo-Roca, Influence of compositionally induced defects on the vibrational properties of device grade $Cu_2ZnSnSe_4$ absorbers for kesterite based solar cells, Applied Physics Letters 106 (2015) 073903.

[36] J.E. Moore, C.J. Hages, R. Agrawal, M.S. Lundstrom, J.L. Gray, The importance of band tail recombination on current collection and open-circuit voltage in CZTSSe solar cells, Applied Physics Letters 109 (2016) 021102.

[37] C.M. Sutter-Fella, J.A. Stückelberger, H. Hagendorfer, F. La Mattina, L. Kranz, S. Nishiwaki, A.R. Uhl, Y.E. Romanyuk, A.N. Tiwari, Sodium Assisted Sintering of Chalcogenides and Its Application to Solution Processed $Cu_2ZnSn(S,Se)_4$ Thin Film Solar Cells, Chemistry of Materials 26 (2014) 1420–1425.

[38] J. Li, J. Huang, J. Cong, Y. Mai, Z. Su, G. Liang, A. Wang, M. He, X. Yuan, H. Sun, C. Yan, K. Sun, N.J. Ekins-Daukes, M.A. Green, X. Hao, Large-Grain Spanning Monolayer $Cu_2ZnSnSe_4$ Thin-Film

Solar Cells Grown from Metal Precursor, Small 18 (2022) 2105044.
[39] W. Jeong, K. Kim, J. Kim, H.K. Park, J. Min, J. Lee, S. Mun, S. Kim, J. Jang, W. Jo, D. Lee, Impact of Na Doping on the Carrier Transport Path in Polycrystalline Flexible $Cu_2ZnSn(S,Se)_4$ Solar Cells, Advanced Science 7 (2020) 1903085.
[40] M. Han, X. Zhang, Z. Zeng, An investigation of Na-related defects in $Cu_2ZnSnSe_4$, Phys. Chem. Chem. Phys. 19 (2017) 17799–17804.
[41] K.-J. Yang, S. Kim, J.-H. Sim, D.-H. Son, D.-H. Kim, J. Kim, W. Jo, H. Yoo, J. Kim, J.-K. Kang, The alterations of carrier separation in kesterite solar cells, Nano Energy 52 (2018) 38–53.
[42] H. Yoo, J.S. Jang, S.W. Shin, J. Lee, J. Kim, D.M. Kim, I.J. Lee, B.H. Lee, J. Park, J.H. Kim, Influence of the Reaction Pathway on the Defect Formation in a $Cu_2ZnSnSe_4$ Thin Film, ACS Appl. Mater. Interfaces 13 (2021) 13425–13433.
[43] D. Son, D. Jeon, D. Kim, J. Kang, S. Sung, J. Lee, T. Lee, E. Enkhbayar, J. Kim, K. Yang, Identifying the relationships between subsurface absorber defects and the characteristics of kesterite solar cells, Carbon Energy 5 (2023) e336.
[44] K. Wang, O. Gunawan, T. Todorov, B. Shin, S.J. Chey, N.A. Bojarczuk, D. Mitzi, S. Guha, Thermally evaporated Cu_2ZnSnS_4 solar cells, Applied Physics Letters 97 (2010) 143508. https://doi.org/10.1063/1.3499284.
[45] S.S. Hegedus, W.N. Shafarman, Thin-film solar cells: device measurements and analysis, Progress in Photovoltaics 12 (2004) 155–176.
[46] Y. Sun, H. Guo, P. Qiu, S. Zhang, S. Wang, L. Wu, J. Ao, Y. Zhang, Na-doping-induced modification of the $Cu_2ZnSn(S,Se)_4$/CdS heterojunction towards efficient solar cells, Journal of Energy Chemistry 57 (2021) 618–626.
[47] B. Liu, J. Guo, R. Hao, L. Wang, K. Gu, S. Sun, A. Aierken, Effect of Na doping on the performance and the band alignment of CZTS/CdS thin film solar cell, Solar Energy 201 (2020) 219–226.
[48] E. Von Hauff, Impedance Spectroscopy for Emerging Photovoltaics, J. Phys. Chem. C 123 (2019) 11329–11346.
[49] X. Cui, K. Sun, J. Huang, J.S. Yun, C.-Y. Lee, C. Yan, H. Sun, Y. Zhang, C. Xue, K. Eder, L. Yang, J.M. Cairney, J. Seidel, N.J. Ekins-Daukes, M. Green, B. Hoex, X. Hao, Cd-Free Cu_2ZnSnS_4 solar cell with an efficiency greater than 10% enabled by Al_2O_3 passivation layers, Energy Environ. Sci. 12 (2019) 2751–2764.

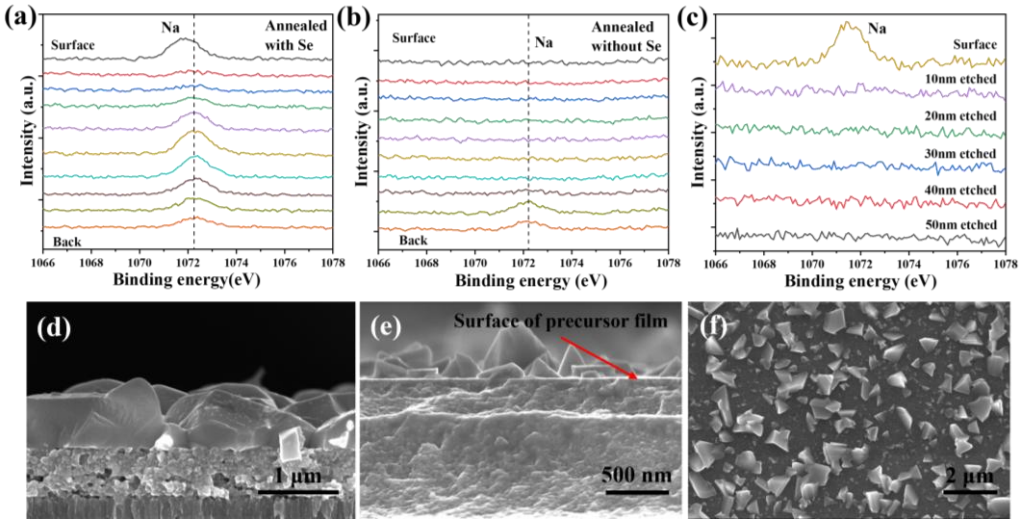

Figure S1. Na XPS depth profiles for precursor films annealed with Se (a) and without Se (b); Na XPS depth profile in the surficial region of the film annealed with Se (c); SEM images of the films after the whole selenization (d) and after the early-stage of the selenization (e,f).

Sodium is usually detected in CZTSSe films even the precursor films are not doped with sodium. For CZTSSe films prepared on sodium lime glass (SLG) substrates, sodium can incorporate in the CZTSSe film by two paths. Firstly, the sodium can diffuse from the SLG substrate to CZTSSe film. Secondly, gaseous $NaSe_x$ can be generated via the reaction between SLG and Se in the selenization process. [1] The condense of the gaseous $NaSe_x$ on the CZTSSe film and the subsequent top-to-down diffusion of the sodium can incorporate sodium in the CZTSSe film. To clarify the origin of sodium in our own CZTSSe films (without Na-doping in the precursor film), we compare the depth Na XPS profiles of the films that annealed with Se (conventional selenization) and without Se (using the same temperature profile as the conventional selenization, but no Se is used during the annealing). For the films annealed without Se, sodium can only enter the film by diffusing from the SLG substrate (the generation of the gaseous $NaSe_x$ is prevented due to the lack of Se). In this condition, the Na XPS peaks can only be detected near the back surface of the film (**Figure S1(b)**). This result indicates that the diffusion of sodium from the SLG substrate can only cause the Na-incorporation at the bottom of the film. For the film selenized with Se, sodium can be detected in the other regions of the film. Since the different films are annealed with the same temperature profile, the diffusion of the sodium from SLG to CZTSSe film could be similar between each other. Therefore, it can be concluded that the formation and condense of the gaseous $NaSe_x$ is the main path for the Na-incorporation

in our own CZTSSe films.

Besides, for almost all the CZTSSe films that characterized by XPS, a thin Na-rich layer (<10nm, Na/(Cu+Zn+Sn) can be above 20%) can be detect on the surface of the film (**Figure S1(c)**), which could result from the condense of the gaseous $NaSe_x$ on the CZTSSe film. Due to the existence of sodium, as well as the Se-rich environment, a thin layer of $NaSe_x$ flux may be generated on the surface of the CZTSSe film in the selenization process. Such liquid flux may assist the growth of the CZTSSe grains by enhancing the elemental diffusion.

After selenization, the CZTSSe film usually exhibits the bi-layer structure which consists of a large-grain layer and a fine-grain layer (**Figure S1(d)**). In this structure, there is usually a flat boundary line between the large-grain layer and the fine-grain layer. It looks like that the large-grain layer "grows" on the fine-grain layer. **Figure S1(e)** and **Figure S1 (f)** show the SEM images of a half-selenized film (at 530 ºC) which contained separated crystalline grains on the film. These images clearly prove that the CZTSSe grains can grow on the film following the bottom-up direction. To support the bottom-up growth of the CZTSSe grains, specific path should exist to facilitate the bottom-to-top elemental diffusion.

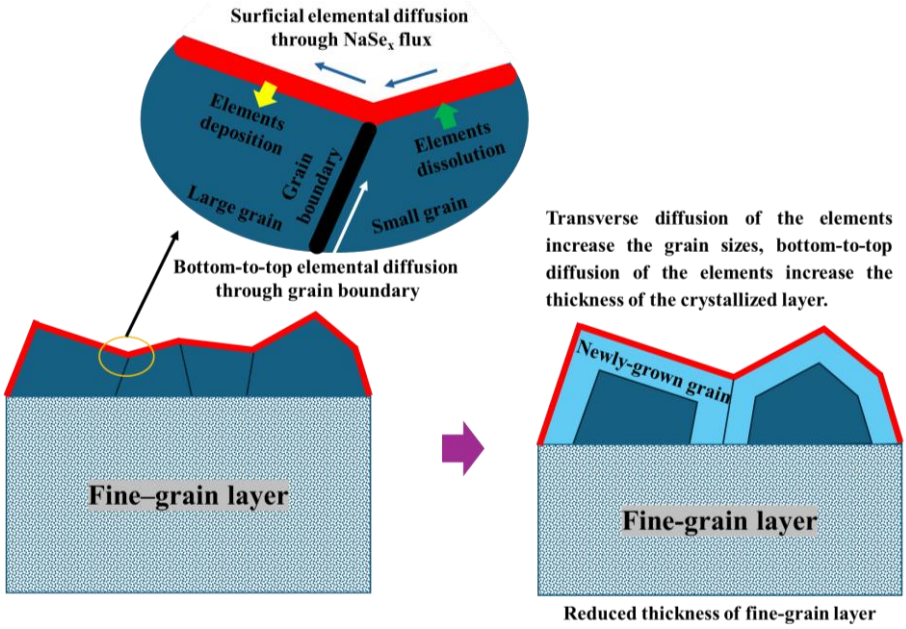

Figure S2. The $NaSe_x$-assisted grain growth in CZTSSe film.

Based on the results and analyses above, a model (Figure S2) is proposed to illustrate the growth of CZTSSe grains at high temperature (>500ºC). As shown in Figure S2, there is a thin crystallized layer on top of the film. In the meanwhile, a thin layer of $NaSe_x$ flux is generated which covers the crystallized layer. Due to the high chemical potential, the elements in small grains of the crystallized layer may dissolve in the $NaSe_x$

flux. Then the elements can transfer and deposit on large grains of the crystalized layer (in which the elements have low chemical potentials) through the $NaSe_x$ flux. Since the $NaSe_x$ flux can significantly enhance the transport of the elements, the rapid growth of the CZTSSe grains can be achieved with the assistance of $NaSe_x$ flux. Besides, it is believed the elements in the bottom fine-grain layer can diffuse to the surface through the grain boundaries of the top crystallized layer. Then the elements can transfer and deposit on large grains of the crystalized layer through the $NaSe_x$ flux. By this process, the thickness of the crystallized layer can be increased. Meanwhile, the thickness of the fine-grain layer could be decreased due to the loss of the elements. Depending on whether the bottom-to-top elemental diffusion through the grain-boundaries is blocked or not, the fine grain layer may remain or disappear after the selenization.

Table S1. Compositions of the CZTSSe films with different selenization conditions.

Sample	Cu (at%)	Zn (at%)	Sn (at%)	Se (at%)	S (at%)	Cu/ (Zn+Sn)	Zn/Sn	S/ (S+Se)
W/O-Na	25.4	16.5	15.6	38.4	4.1	0.79	1.06	0.10
W-NaCl	26.2	15.6	16.4	39.4	2.5	0.82	0.95	0.06
W-NaF	26.9	15.8	15.9	39.0	2.4	0.85	0.99	0.06
W-NaOH	26.0	17.6	15.3	38.8	2.4	0.79	1.15	0.06
W-$Na_2S_2O_3$	26.0	17.8	15.2	39.0	2.1	0.79	1.17	0.05
W-Na_2S	27.4	16.6	15.0	39.2	1.8	0.87	1.11	0.04

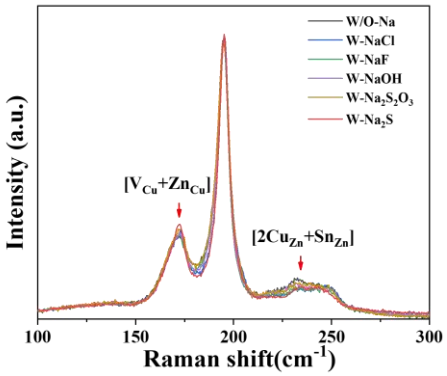

Figure S3. Normalized Raman spectra of the CZTSSe films with different selenization conditions.

Compared to the Raman spectrum of the W/O-Na film, the Raman spectra of the co-selenized CZTSSe films exhibit stronger peak at 170 cm^{-1} and reduced intensities at around 185 cm^{-1} and 220 cm^{-1} (especially for the W-Na_2S film). While the enhanced Raman peak at 170cm^{-1} indicated that the concentration of the

Zn_{Cu} defect is decreased in CZTSSe film, the reduced intensity at around 185 cm^{-1} and 220 cm^{-1} implied that the concentration of the Sn_{Zn} defect is decreased in CZTSSe film. [2] As Zn_{Cu} and Sn_{Zn} defects can cause donner level and deep level in the energy structure of CZTSSe, the reduced Zn_{Cu} and Sn_{Zn} defects would be beneficial to the electrical quality of the CZTSSe film.

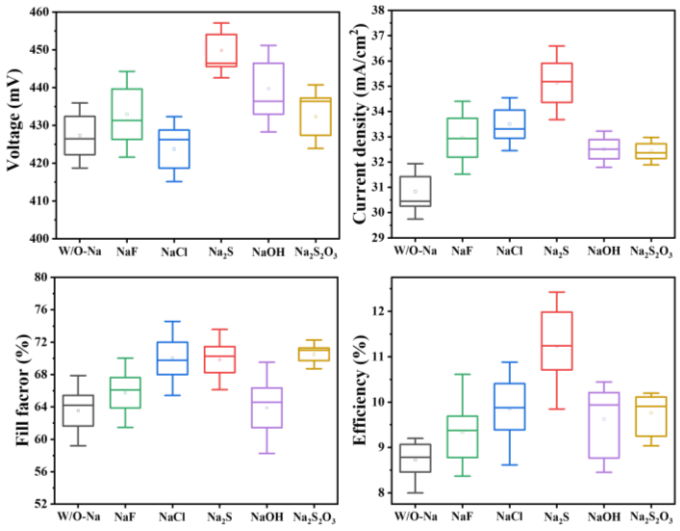

Figure S4. Parameter statistics for solar cells with different selenization processes

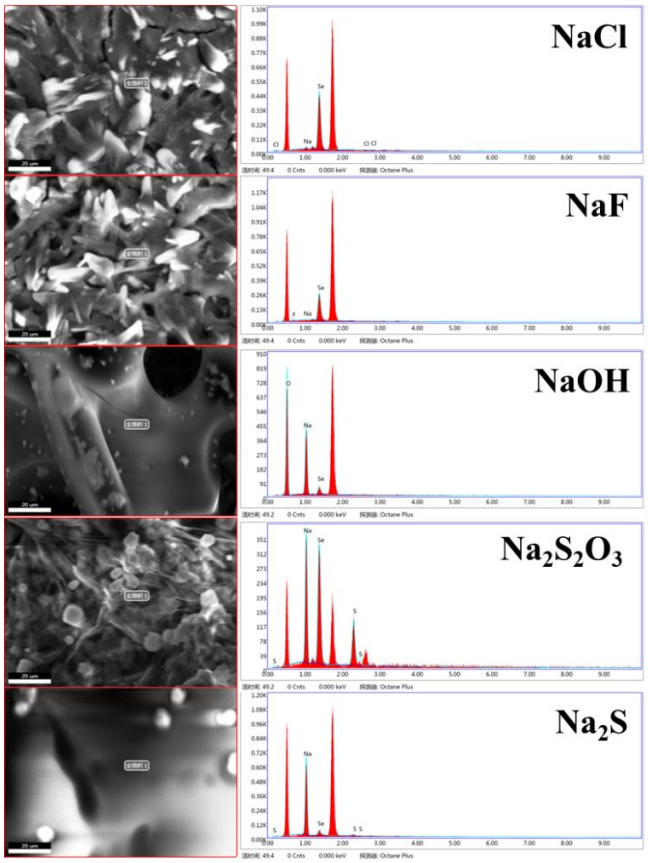

Figure S5. Morphologies and EDS spectra for the residues of the sodium sources after selenization.

Table S2. Compositions for the residues of the sodium sources.

Sample	Na (at%)	Se (at%)	X(Cl/F/O/S) (at%)
NaCl	4.9	91.7	3.3
NaF	2.8	80.3	16.9
NaOH	35.3	1.5	63.2
$Na_2S_2O_3$	56.3	36.6	9.1
Na_2S	94.7	3.7	1.7

Figure S4 and **Table S2** shows the EDS results for the residues of the sodium sources after selenization. For the NaCl and NaF source, only weak Na peak can be detected in the EDS spectra, indicated that most of the sodium in NaCl/NaF are lost after selenization. Since NaCl and NaF are not volatile substance at the selenization temperature, the loss of sodium could be caused by the formation of volatile $NaSe_x$ (via the reaction between NaCl/NaF and Se) in the selenization processes. These results imply that the reaction between Se and NaCl/NaF could be easier than the other sodium sources. For the $Na_2S_2O_3$ source, the EDS spectrum of the residue exhibits stronger Na and Se peaks, indicated that the generation of gaseous $NaSe_x$ may be difficult by the reaction between $Na_2S_2O_3$ and Se. For the NaOH source, stronger O peak (partly result from the quartz substate) can be observed in the EDS spectra of the residue. The residual O in the NaOH source may affect the generation and the properties of the gaseous $NaSe_x$. For the Na_2S source, obvious Na peak can be detected in the EDS spectra of the residue, but the Se peak is quite weak. The differences suggest that the reaction between the sodium sources and Se, as well as the generation of the gaseous $NaSe_x$ are different among the co-selenization processes.

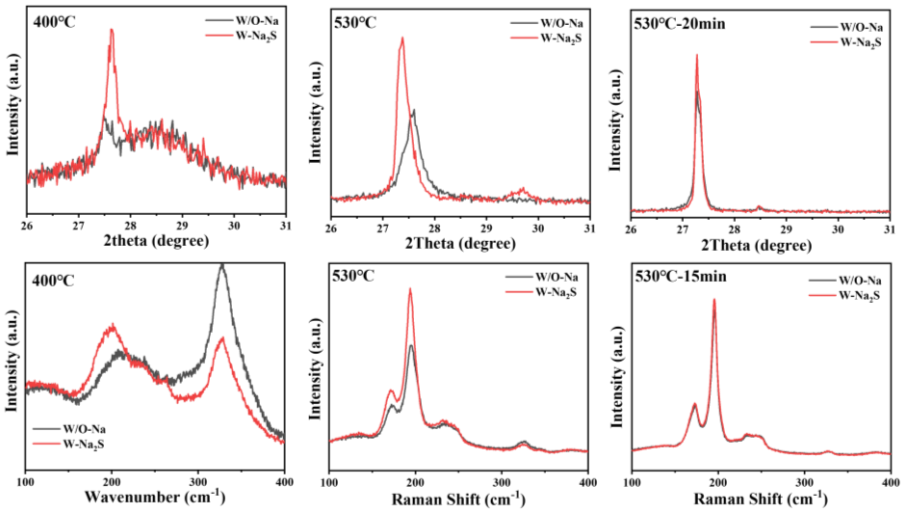

Figure S6. Enlarged XPD patterns and Raman spectra for the half-selenized W/O-Na and W-Na_2S films at different temperatures.

Table S3. Compositions of the half-selenized W/O-Na films at different temperatures.

	300℃	350℃	400℃	450℃	500℃	530℃	530℃/15min
CuL	19.7	19.6	19.5	22.5	24.4	25.3	27.1
SnL	12.4	13.1	12.6	13.9	14.6	15.0	15.7
ZnL	13.5	13.3	12.6	11.3	15.1	15.5	15.6
SeL	0.3	3.3	19.9	29.7	35.6	38.1	37.6
SL	54.2	50.8	35.4	22.6	10.4	6.1	4.0
Cu/(Sn+Zn)	0.76	0.74	0.77	0.89	0.82	0.83	0.87
Zn/Sn	1.09	1.02	1.00	0.81	1.03	1.04	0.99
S/(S+Se)	0.99	0.94	0.64	0.43	0.23	0.13	0.10

Table S4. Compositions of the half-selenized W-Na_2S films at different temperatures.

	300℃	350℃	400℃	450℃	500℃	530℃	530℃/15min
CuL	20.8	19.2	18.4	23.3	26.2	24.3	27.4
SnL	11.4	12.0	13.0	14.6	14.3	15.8	15.0
ZnL	12.4	13.1	13.2	10.2	14.1	17.1	16.6
SeL	1.4	4.7	23.4	29.9	36.1	39.2	39.2
SL	54.1	51.0	32.1	22.0	9.4	3.4	1.8
Cu/(Sn+Zn)	0.88	0.76	0.70	0.94	0.92	0.73	0.86
Zn/Sn	1.09	1.09	1.02	0.69	0.98	1.09	1.11
S/(S+Se)	0.98	0.92	0.58	0.42	0.21	0.08	0.04

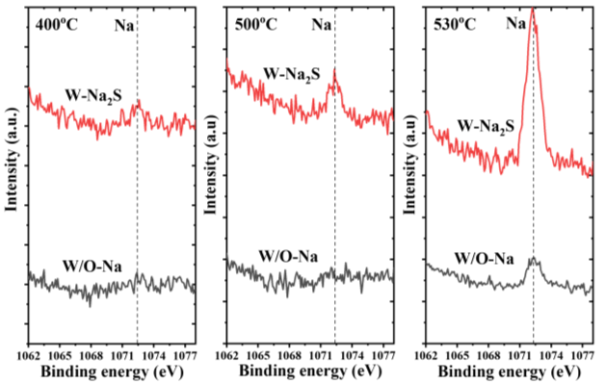

Figure S7. XPS characterization results on the surface of the half selenized films at different temperatures.

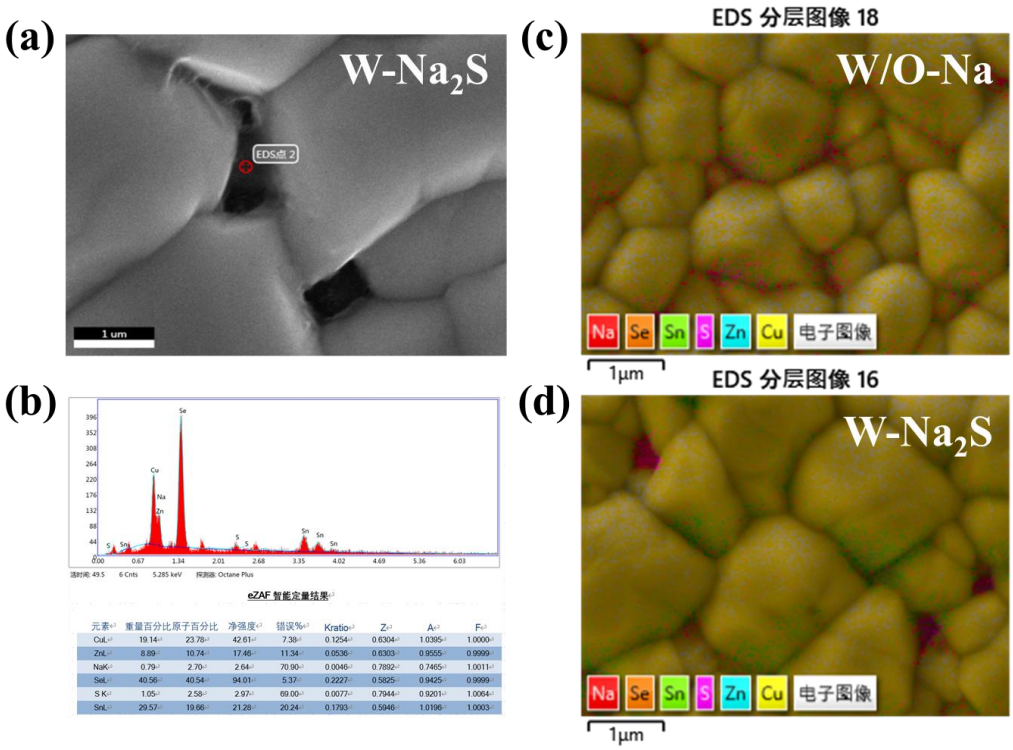

Figure S8. (a,b) SEM images and spot EDS results of W-Na_2S film; (c,d) EDS mapping of W/O-Na and W-Na_2S films.

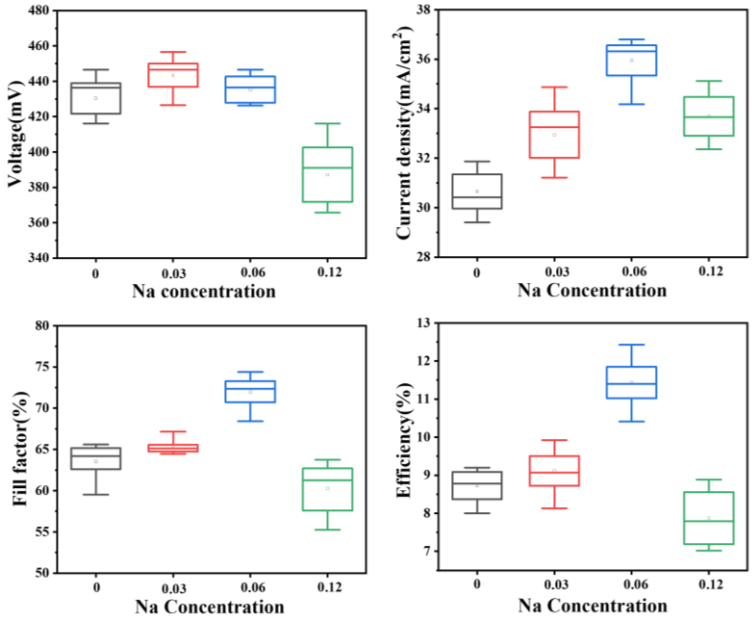

Figure S9. Variation of the solar cell performances as the concentration of the Na_2S aqueous solution.

The quantity of the sodium source used for the co-selenization is adjusted by changing the concentration of the aqueous solution. Generally, more sodium source is loaded on the quartz slide when high concentration solution is used. The concentration of the aqueous solution is optimized by using Na_2S as sodium source. **Figure S9** shows the variation of the solar cell parameters as the concentration of the Na_2S solution. It is proved that the solar cell achieves the best efficiency when the concentration of the Na_2S solution is 0.06

mol/L. For comparison, the concentrations for all the aqueous solutions (contained different sodium sources) are fixed at 0.06 mol/L.

References

[1] T. Abzieher, T. Schnabel, M. Hetterich, M. Powalla, E. Ahlswede, Phys. Status Solidi A **2016**, *213*, 1039.

[2] M. Dimitrievska, A. Fairbrother, E. Saucedo, A. Pérez-Rodríguez, V. Izquierdo-Roca, Appl. Phys. Lett. **2015**, *106*, 073903.